Journal of Nanobiotechnology

RESEARCH

Open Access

Probiotic membrane vesicles ameliorate atherosclerotic plaques by promoting lipid efflux and polarization of foamy macrophages

Boping Jing[1,2,3†], Yu Gao[3,4†], Lufang Wang[1,2,3†], Feng Guo[5], Dawei Jiang[3,4], Saimei Qin[1,2,3], Mengrong He[1,2,3], Ying Bai[1,2,3], Rui An[3,4], Mingxing Xie[1,2,3*] and Li Zhang[1,2,3*]

Abstract

Foamy macrophages are pivotal contributors to the development and progression of atherosclerotic plaques, posing a substantial threat to human health. Presently, there is no pharmaceutical intervention available to effectively eliminate foamy macrophages. In this study, we demonstrate that probiotic membrane vesicles (MVs) can induce atherosclerotic plaque regression by modulating foamy macrophages. MVs isolated from *Lactobacillus rhamnosus* exhibited a specific uptake by foamy macrophages. Near-infrared fluorescence (NIRF) imaging, aortic oil red O staining, and hematoxylin and eosin staining showed reductions in the plaque area following MVs treatment. Mechanistically, bioinformatics analysis provided insights into how MVs exert their effects, revealing that they promote lipid efflux and macrophage polarization. Notably, MVs treatment upregulated *NR1H3*, which in turn increased *ABCA1* expression, facilitating lipid efflux from foamy macrophages. Moreover, MVs shifted macrophage polarization from a pro-inflammatory M1 phenotype to an anti-inflammatory M2 phenotype, highlighting their potential to create a more protective environment against plaque progression. This study is significant as it introduces MVs as a novel therapeutic platform for the targeted delivery of anti-inflammatory agents to atherosclerotic sites. By specifically modulating macrophage function, MVs hold considerable potential for the treatment of atherosclerosis and related cardiovascular diseases, addressing an unmet need in current therapeutic strategies.

Graphical Abstract

Schematic diagram of probiotic membrane vesicles (MVs)-mediated atherosclerotic plaque regression and the mechanism by which foamy macrophages are regulated. The mechanism reveals two pivotal findings: the promotion of lipid efflux and the polarization of macrophages.

†Boping Jing, Yu Gao and Lufang Wang contributed equally to this work.

*Correspondence:
Mingxing Xie
xiemx@hust.edu.cn
Li Zhang
zli429@hust.edu.cn

Full list of author information is available at the end of the article

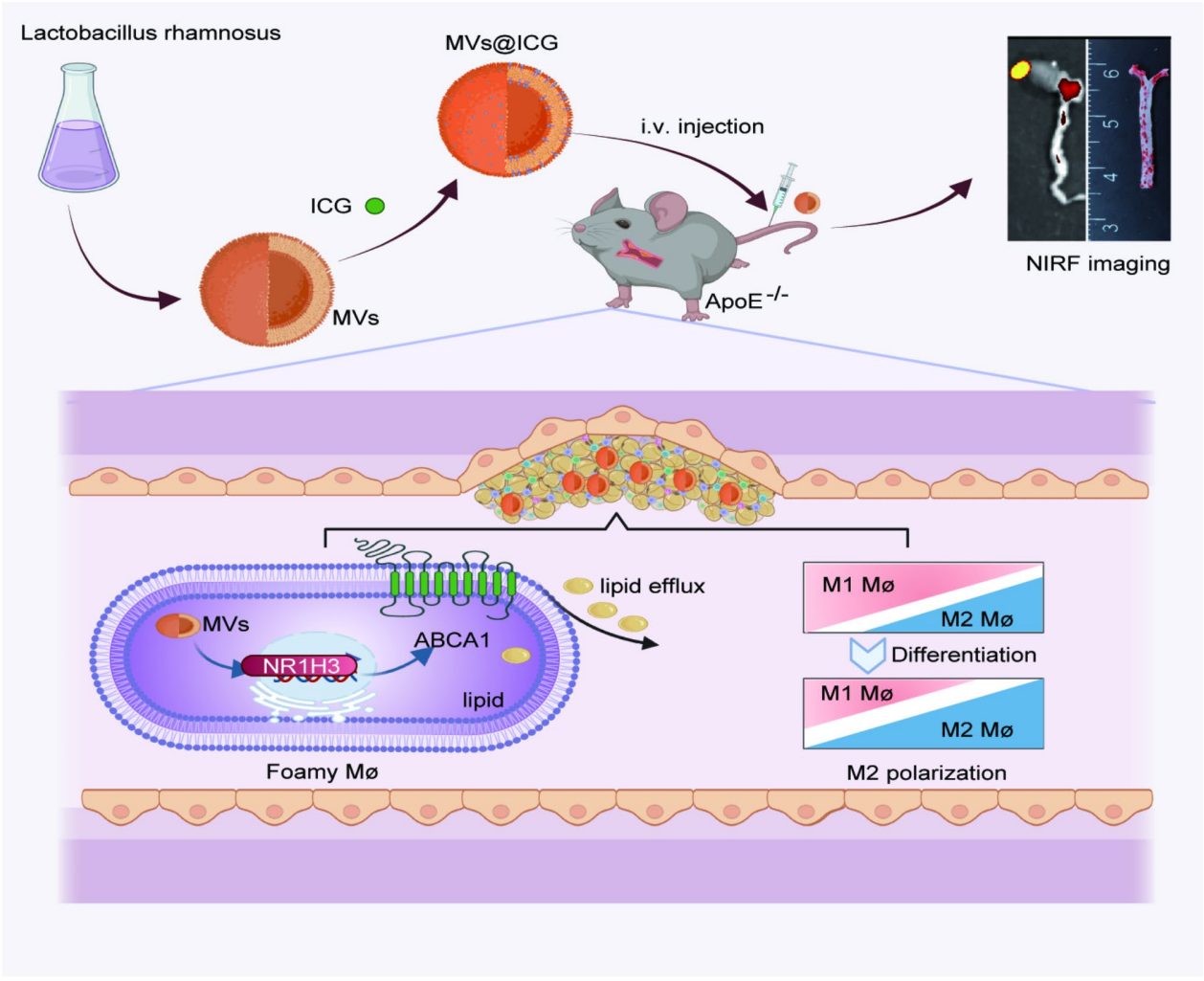

Keywords Probiotic membrane vesicles, Foamy macrophages, Lipid metabolism, Atherosclerosis

Introduction

Cardiovascular disease is a leading cause of death worldwide, and the instability and rupture of atherosclerotic plaques are primary contributors to mortality in these patients [1, 2]. Despite the availability of pharmacological treatments, they have proven inadequate in effectively managing the rising prevalence and associated mortality of cardiovascular diseases [3, 4]. This situation underscores the urgent need for new, safe, and effective therapies to halt or reverse the progression of atherosclerosis (AS).

A critical aspect of atherosclerotic plaque development is the accumulation of foamy macrophages, which are key players in the pathogenesis of AS. These cells contribute to the formation and growth of plaques, weakening the fibrous cap, and enlarging the necrotic core, all of which increase the risk of plaque rupture and subsequent thrombosis [5]. Therefore, mitigating lipid deposition in foamy macrophages is a promising therapeutic strategy for addressing atherosclerosis [6, 7].

Targeted drug delivery is emerging as an ideal approach for treating AS, and it has become a focal point of current research [8–12]. Extracellular vesicles have emerged as highly promising nanocarriers and are presently under investigation in various clinical trials [13–19]. The specific functions of extracellular vesicles depend on their origins. Specifically, membrane vesicles (MVs) derived from probiotics, such as Lactobacillus rhamnosus, have demonstrated notable anti-inflammatory and immunomodulatory properties [20, 21]. Prior investigations have revealed that MVs induce the secretion of the anti-inflammatory cytokine interleukin (IL)-10, as well as the immunomodulatory cytokines IL-1β and granulocyte-macrophage colony-stimulating factor (GM-CSF). These

actions help restore the balance between pro-inflammatory M1 and anti-inflammatory M2 macrophages, which is crucial in controlling inflammation and improving outcomes in immune-related conditions [22, 23].

Given these well-documented anti-inflammatory properties, we hypothesized that MVs could serve as an effective therapeutic strategy for atherosclerosis by specifically targeting foamy macrophages. This hypothesis is grounded in the unique potential of MVs to modulate immune responses and alter foamy macrophage behavior, thereby addressing a critical aspect of AS progression.

To explore this novel application, we conducted a series of in vitro and in vivo experiments, marking the first time MVs have been applied in AS. MVs were isolated from *Lactobacillus rhamnosus* and thoroughly characterized for their ability to target and regulate foamy macrophages. In vitro studies were conducted to assess the impact of MVs on macrophage function and lipid metabolism. In vivo AS models were used to evaluate the accumulation of MVs within atherosclerotic plaques and their subsequent effects on plaque progression and stability. Furthermore, the underlying mechanisms were investigated through RNA-sequencing and biological experiments. The significance of this study lies in its potential to introduce a groundbreaking approach to the treatment of AS. Our study could pave the way for new therapeutic avenues that leverage the natural properties of MVs, offering a safer and more targeted alternative to conventional treatments.

Methods

Cell culture and foamy macrophage induction

Human THP-1 cells were acquired from the American Type Culture Collection (ATCC; Manassas, VA, USA) and seeded in 35 mm Petri dishes at a density of 0.5 × 10^6 cells/mL. The cells were cultured in RPMI 1640 medium supplemented with 10% FBS, 10 IU/mL penicillin, and 10 μg/mL streptomycin. The cells were maintained at 37 °C in a humidified atmosphere containing 5% CO_2. To induce macrophage differentiation, THP-1 cells were treated with 100 ng/mL phorbol 12-myristate 13-acetate (PMA) for 48 h. Subsequently, the macrophages were transformed into foamy macrophages by incubation with 50 μg/mL oxidized low-density lipoprotein (oxLDL) in serum-free RPMI 1640 medium supplemented with 0.3% BSA for 48 h.

Animals

The animal protocol received approval from the Animal Care Committee of Tongji Medical College, Huazhong University of Science and Technology. Male $ApoE^{-/-}$ mice (aged 6 weeks) were procured from Beijing Vital River Laboratory Animal Technology Co., Ltd, China and were subsequently housed in a specific pathogen-free environment. Additionally, 6-week-old female C57BL/6 mice were obtained from Beijing HFK Bioscience Co., Ltd, China, and housed in a specific pathogen-free environment.

Preparation of *Lactobacillus rhamnosus*-derived MVs

Lactobacillus rhamnosus was procured from BeNa Culture Collection (BNCC136673, China) and cultured in Man-Rogosa-Sharpe (MRS) medium. The bacteria were harvested after 48 h, washed with PBS, and then stored at -20 °C in 1.1 ml aliquots, each containing 1 × 10^10 colony-forming units (CFUs)/ml. membrane vesicles (MVs) were extracted from *Lactobacillus rhamnosus* MRS broth culture after 48 h. Following centrifugation at 600 × g for 30 min, the supernatants underwent two successive washes with PBS and centrifugation at 100,000 × g at 4 °C. The resultant MVs were resuspended in PBS, filtered through 0.22 μm filters (Millipore, USA), and stored at -80 °C in PBS. MVs quantification was carried out with a BCA Protein Assay Kit (Beyotime, Shanghai, China), and the samples were preserved at – 80 °C.

Characterization of MVs

The examination of MVs involved the use of a transmission electron microscope (TEM) from Hitachi, Japan, and dynamic light scattering (DLS) was performed with equipment from Malvern Instruments Ltd., Worcestershire, UK. To assess the in vitro stability of MVs, hydrodynamic diameters were monitored over 7 days with DLS.

In vitro cell uptake assay

In vitro cell binding was assessed by flow cytometry and confocal imaging. Dimethyl sulfoxide (DMSO, Solarbio, China) was used to enhance the solubility and permeability of indocyanine green (ICG, Sigma-Aldrich) across the MVs lipid membrane. A solution consisting of 4% (v/v) DMSO in normal saline (NS) was used to encapsulate ICG. Subsequently, MVs@ICG was produced by blending MVs with ICG and incubating the mixture for 6 h with agitation in the dark at 4 °C. The resulting samples were purified using PDG-25 desalting columns and stored at 4 °C for future use. MVs@ICG was incubated with macrophages or foamy macrophages at 37 °C for varying times (0, 1, 6, and 12 h) and at different concentrations (0, 1, 5, 10, and 20 μg/mL). Flow cytometry was used to detect fluorescence signals. Additionally, MVs@ICG (ICG 5 μg/mL) and ICG (5 μg/mL) were incubated with macrophages or foamy macrophages at 37 °C for 24 h. Cell nuclei were stained with 4′,6-diamidino-2-phenylindole (DAPI, Boster, Wuhan, China), and the cytoskeleton was stained with FITC-phalloidin (Proteintech, Wuhan, China). The fixed cells were then observed using a confocal microscope (Leica, Germany).

Ex vivo near-infrared fluorescence (NIRF) imaging

$ApoE^{-/-}$ mice were subjected to a high-fat diet regimen for 4 months and were randomly divided into two groups. For NIRF imaging, MVs@ICG and ICG were separately administered via tail vein injections to each group of mice ($n = 3$). The mice were anaesthetized with 2% isoflurane, and their hearts and aortas were meticulously extracted at various time points (1, 2, and 3 h). Static NIRF images were acquired using the IVIS Spectrum imaging system (PerkinElmer, USA) with 750 nm excitation and 790 nm emission filters. Additionally, ex vivo NIRF imaging of major organs was conducted.

Treatment protocol

To assess the impact of MVs on the regression of atherosclerotic plaques, male $ApoE^{-/-}$ mice were subjected to a high-fat diet for 4 weeks and subsequently randomly divided into 2 groups, each consisting of 5 mice. In the MVs group, $ApoE^{-/-}$ mice were administered MVs (25 mg/kg) via injection once per week for a total of 8 weeks. Conversely, the control group mice received PBS injections once per week for the same 8-week period. In the 18th week, all $ApoE^{-/-}$ mice were administered MVs@ICG and subsequently euthanized for further analysis.

Blood analysis and haematological parameters

Blood samples were collected in ethylenediaminetetraacetic acid spray-coated tubes, and haematological parameters were promptly analysed using an automated haematology analyser (Sysmex KX-21, Sysmex Co., Japan). This analysis included red blood cells (RBCs), white blood cells (WBCs), platelets (PLTs), haemoglobin (HGB), haematocrit (HCT), mean corpuscular volume (MCV), mean corpuscular haemoglobin (MCH), and mean corpuscular haemoglobin concentration (MCHC).

Biochemical analysis of plasma parameters

Plasma concentrations of various biochemical parameters, including alanine aminotransferase (ALT), aspartate aminotransferase (AST), alkaline phosphatase (ALP), creatinine (CRE), blood urea nitrogen (BUN), high-density lipoprotein cholesterol (HDL-C), low-density lipoprotein cholesterol (LDL-C), triglycerides (TG), and total cholesterol (T-CHO), were quantified using an automated analyser (Roche Cobas C501, Roche Co., Switzerland).

Histological and immunostaining analysis

The entire aorta was isolated from $ApoE^{-/-}$ mice and subjected to oil red O staining. Atherosclerotic lesions were assessed using haematoxylin and eosin (H&E) staining, and the plaque and lumen areas were quantified separately under a microscope. To evaluate lipid content within plaques, oil red O staining or Sudan IV staining of arterial cryosections was conducted. Masson's trichrome staining was used to determine the collagen content of atherosclerotic plaques. Immunohistochemistry (IHC) and immunofluorescence staining were also carried out. Furthermore, major organs, including the heart, liver, spleen, lungs, and kidneys, were subjected H&E staining and subsequently examined using an optical microscope (IX73, Olympus, Japan).

RNA sequencing of foamy macrophages

THP-1 cells were stimulated with phorbol 12-myristate 13-acetate (PMA, 100 ng/mL) for 48 h, followed by incubation with oxLDL (50 μg/mL) for an additional 48 h to induce the formation of foamy macrophages. Subsequently, RNA was isolated from foamy macrophages treated with or without MVs (10 μg/mL) using TRIzol reagent (#15596026, Invitrogen). Transcriptome sequencing was conducted by NOVOGENE (Beijing, China) using the Illumina platform. The prepared libraries were sequenced on an Illumina NovaSeq platform to generate 150-bp paired-end reads.

Western blot analysis

Cells in the THP-1, THP-1 + PMA (TP), THP-1 + PMA + oxLDL (TO), and THP-1 + PMA + oxLDL + MVs (TV) groups were harvested and lysed using lysis buffer containing phosphatase inhibitors and 1% protease and kept on ice for 30 min. Subsequently, the cell lysates were centrifuged at 12,000 × g for 15 min at 4 °C, and the resulting supernatants were collected. Protein concentrations were determined with a protein quantification kit (#P0012S, Beyotime). The samples were then transferred onto PVDF membranes, which were blocked with 5% nonfat milk for 1 h at room temperature. then, the membranes were incubated with primary antibodies overnight at 4 °C. On the next day, the membranes were washed with 1x TBST for 30 min and subsequently exposed to the indicated secondary antibodies for 1 h. Next, the membranes were washed three times with PBS and exposed to X-ray films using ECL detection reagents (#WP20005, Thermo Fisher). The antibodies used in this experiment were as follows: *NR1H3* antibody (#14351-1-AP, 1:1000), *CD86* antibody (#13395-1-AP, 1:1000), *CD206* antibody (#60143-1-Ig, 1:1000), and *CD68* antibody (#25747-1-AP, 1:1000), all of which were procured from Proteintech. The *GAPDH* antibody (#ab8245, 1:3000) was obtained from Abcam, and the *ABCA1* antibody (#54186, 1:1000) was sourced from Signalway Antibody.

Quantitative RT–qPCR

Total RNA was extracted using TRIzol reagent (#15596026, Invitrogen). Subsequently, the extracted RNA samples were subjected to reverse transcription

using a PrimeScriptTM RT reagent kit (#RR047A, TAKARA, JPN). Quantitative real-time PCR was performed with a TB GreenTM Fast qPCR Mix kit (#RR430A, TAKARA, JPN). GAPDH was used as the reference gene, and the $2^{-\Delta\Delta CT}$ method was used to calculate the fold change in gene expression. The primer sequences for RT−qPCR are listed in Table S1.

RNA interference

SiControl and gene-specific siRNA were procured from Sigma−Aldrich. THP-1 cells were transfected with siControl or siRNA using Lipofectamine 2000 (#11668019, Thermo Fisher). Twelve hours posttransfection, the transfection medium was replaced with DMEM containing 10% FBS. The siRNA sequences are listed in in Supplementary Data 1 (Table S2).

Bioinformatic analysis

Bioinformatics analyses were conducted by R Bioconductor. To assess differential gene expression and compute average gene values, the robust DESeq2 package was used. Data visualization was achieved by crafting volcano plots and revealing underlying patterns through heatmaps using the ggplot2 [24] and pheatmap packages, respectively. Furthermore, to determine the enriched biological pathways and the functional implications of the changes in gene expression, a comprehensive gene set enrichment analysis (GSEA) was performed by the ClusterProfiler package. To succinctly encapsulate and visually represent the enriched gene ontologies, Gocircle plots were prepared and were underpinned by the GOplot package. These integrated bioinformatics tools and packages collectively enhanced the depth and clarity of our data analysis, ensuring a robust and comprehensive examination of the genetic landscape in our study.

Statistical analysis

Statistical analyses were performed using unpaired or paired Student's t tests for intergroup comparisons, and one-way ANOVA or two-way ANOVA was used for multiple comparisons. Statistical significance was determined using GraphPad Prism 8 software (GraphPad Software, Inc.). $P < 0.05$ was considered statistically significant. The data are expressed as the mean ± standard deviation.

Results

Identification of MVs

MVs were isolated from *Lactobacillus rhamnosus* MRS broth cultures, and the isolation protocol is shown in Fig. 1A. Transmission electron microscopy (TEM) revealed the irregular spherical morphology of MVs. Dynamic light scattering (DLS) analysis indicated that the isolated MVs had a mean diameter of 149.67 ± 2.90 nm (Fig. 1B). Notably, the average hydrodynamic diameter and zeta potential of the MVs remained relatively stable for up to 7 days, demonstrating their remarkable stability (Fig. 1C and D). As shown in Figure S1, macrophages were successfully induced, as indicated by the expression of CD68. Similarly, foamy macrophages were successfully induced, exhibiting the expression of both common markers, CD68 and CD36. To facilitate flow analysis and confocal experiments, ICG was loaded into the MVs (Fig. 1E). The fluorescence signal intensity increased in macrophages (THP-1 + PMA) and foamy macrophages (THP-1 + PMA + oxLDL) with increasing concentrations of MVs@ICG, peaking in response to 5 μg/mL (Fig. 1F and H). Additionally, the fluorescence signal increased with prolonged incubation time in macrophages and foamy macrophages (Fig. 1G and I). Notably, foamy macrophages exhibited higher fluorescence signals than macrophages, which was consistent with the results observed in the confocal images (Fig. 1J).

MVs targeting of atheromatous plaques in atherosclerotic mice

To investigate the targeted delivery of MVs to atheromatous plaques, $ApoE^{-/-}$ mice ($n = 3$) were intravenously administered MVs@ICG and ICG separately via their tail veins. Subsequently, the mice were euthanized at different times (1, 2, and 3 h), and the heart and aorta were collected for NIRF imaging (Fig. 2A). In comparison to the free ICG-treated group, the MVs@ICG-treated group exhibited markedly stronger fluorescence signals in aortic tissues and aortic root sections (Fig. 2B and D). Histological analyses, including oil red staining of aortic tissue and oil red staining combined with H&E staining of aortic root sections, confirmed the successful establishment of the atherosclerosis model, and similar plaque areas were observed in both groups. Notably, as shown in Fig. 2E, the fluorescence signal of ICG correlated with the distribution of the macrophage marker F4/80 in the MVs@ICG-treated group. These findings demonstrate the effective targeting and delivery of MVs to atheromatous plaques, offering valuable insights into potential therapeutic applications.

Therapeutic effects on atherosclerotic plaque development

To assess the therapeutic impact of various treatment protocols on atherosclerotic plaque development, we conducted a comprehensive analysis (Fig. 3A). Aortic specimens were obtained and subjected to NIRF imaging. Notably, aortas from the MVs-treated group exhibited reduced fluorescence intensities compared to those from the control group (Fig. 3B). This observation was further corroborated by quantitative fluorescence analysis (Fig. 3C). Subsequently, aortic specimens were subjected

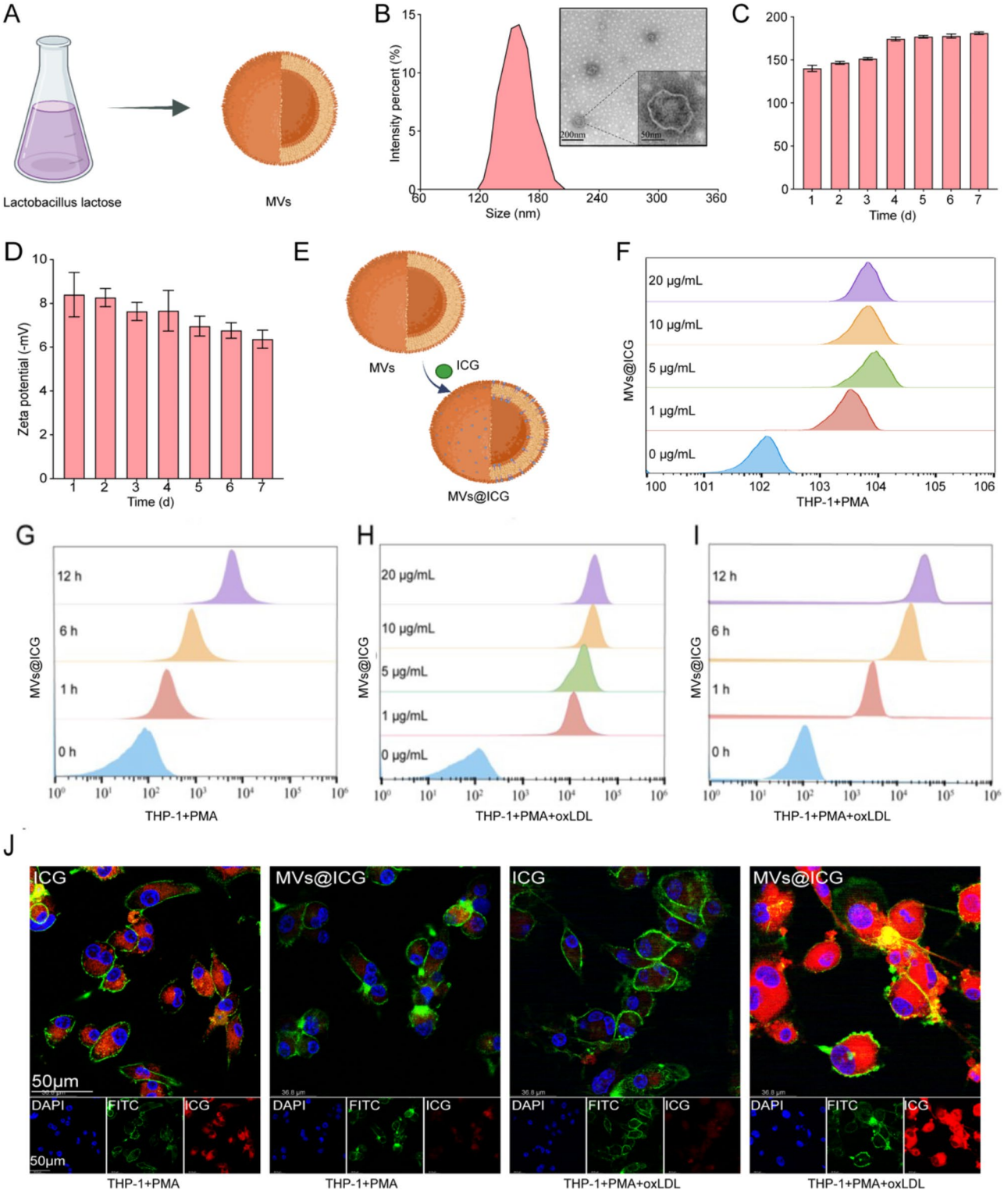

Fig. 1 Characterization of MVs. (**A**) Schematic representation of isolated MVs. (**B**) TEM images and hydrodynamic diameters of MVs. (**C**) The average hydrodynamic diameters of MVs in normal saline over a 7-day period ($n = 3$). (**D**) The average zeta potentials of MVs in normal saline over a 7-day period ($n = 3$). (**E**) Schematic illustration of MVs loaded with ICG. (**F-I**) Flow analysis of different concentrations of MVs@ICG incubated with THP-1 + PMA or THP-1 + PMA + oxLDL for varying times. (**J**) Confocal imaging of MVs@ICG or ICG incubated with THP-1 + PMA or THP-1 + PMA + oxLDL. Cell nuclei were stained with DAPI, and the cytoskeleton was stained with FITC-phalloidin. ($n = 3$, scale bar = 50 μm)

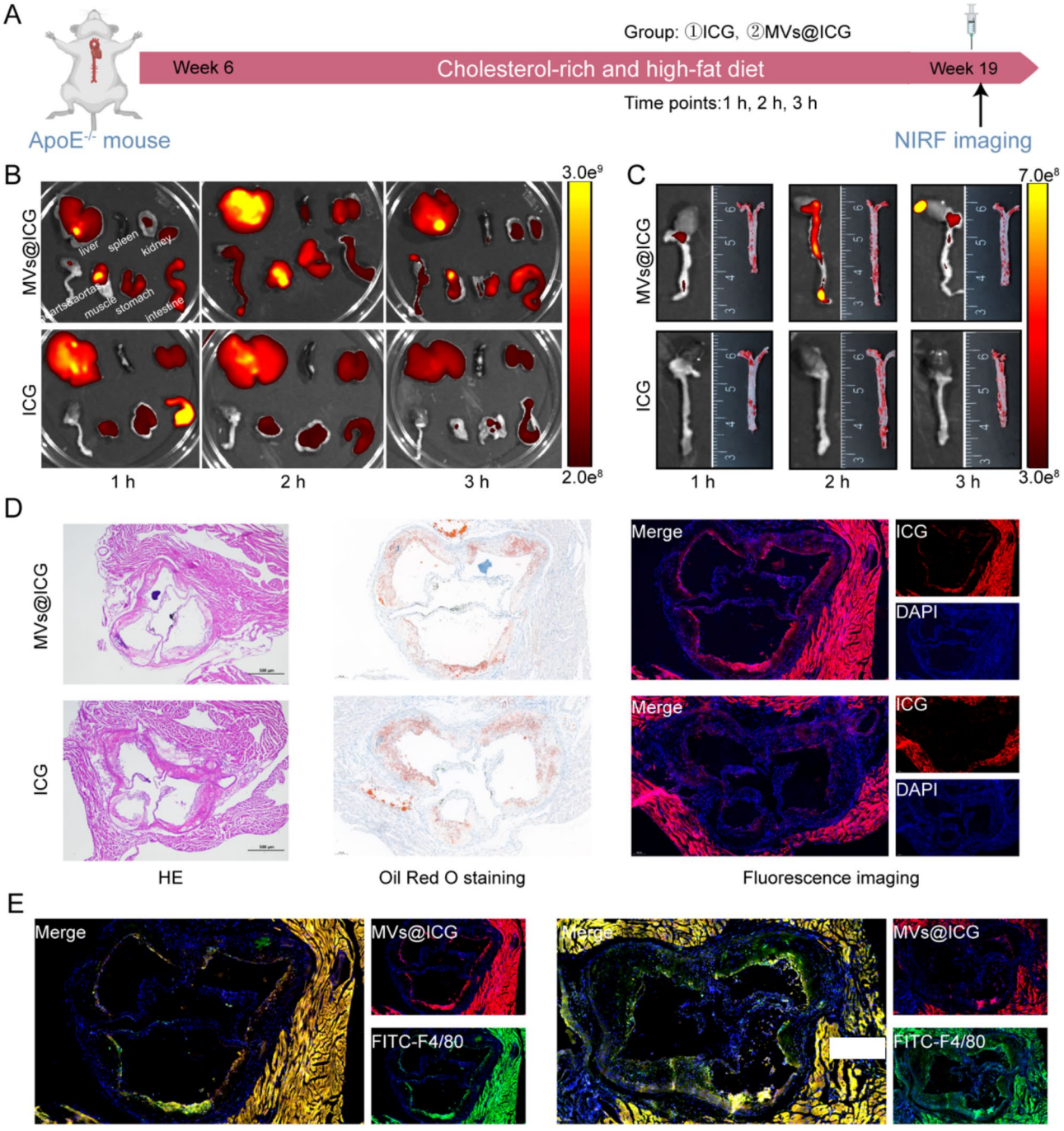

Fig. 2 Targeted delivery of MVs in atherosclerotic mice. (**A**) Schematic representation of the preparation and imaging of atherosclerotic mice. (**B**) Representative ex vivo NIRF images of various tissues at different time points after tail vein injection of ICG or MVs@ICG. (**C**) Representative ex vivo NIRF images and oil red O staining of aortic tissues at different time points after tail vein injection of ICG or MVs@ICG. (**D**) HE staining and oil red O staining of atherosclerotic lesions and fluorescence images showing the accumulation of ICG in the atherosclerotic plaques of ApoE$^{-/-}$ mice injected with ICG or MVs@ICG. (**E**) Immunofluorescence staining of atherosclerotic lesions after tail vein injection of MVs@ICG; nuclei and macrophages were stained with DAPI and FITC-labelled F4/80, respectively. ($n = 3$, scale bar = 200 μm)

to oil red O staining, and the resulting red regions served as indicators of plaque areas (Fig. 3D). We also performed histological and immunohistochemical examinations of aortic root sections containing atherosclerotic plaques. As shown in Fig. 3E, F, H, amp and E and oil red O staining showed the presence of multiple plaques, and there was a significant reduction in the plaque area in the MVs-treated group (Fig. 3G). Additionally, the control group exhibited more pronounced ICG fluorescence than the other group (Fig. 3H). Furthermore, we assessed

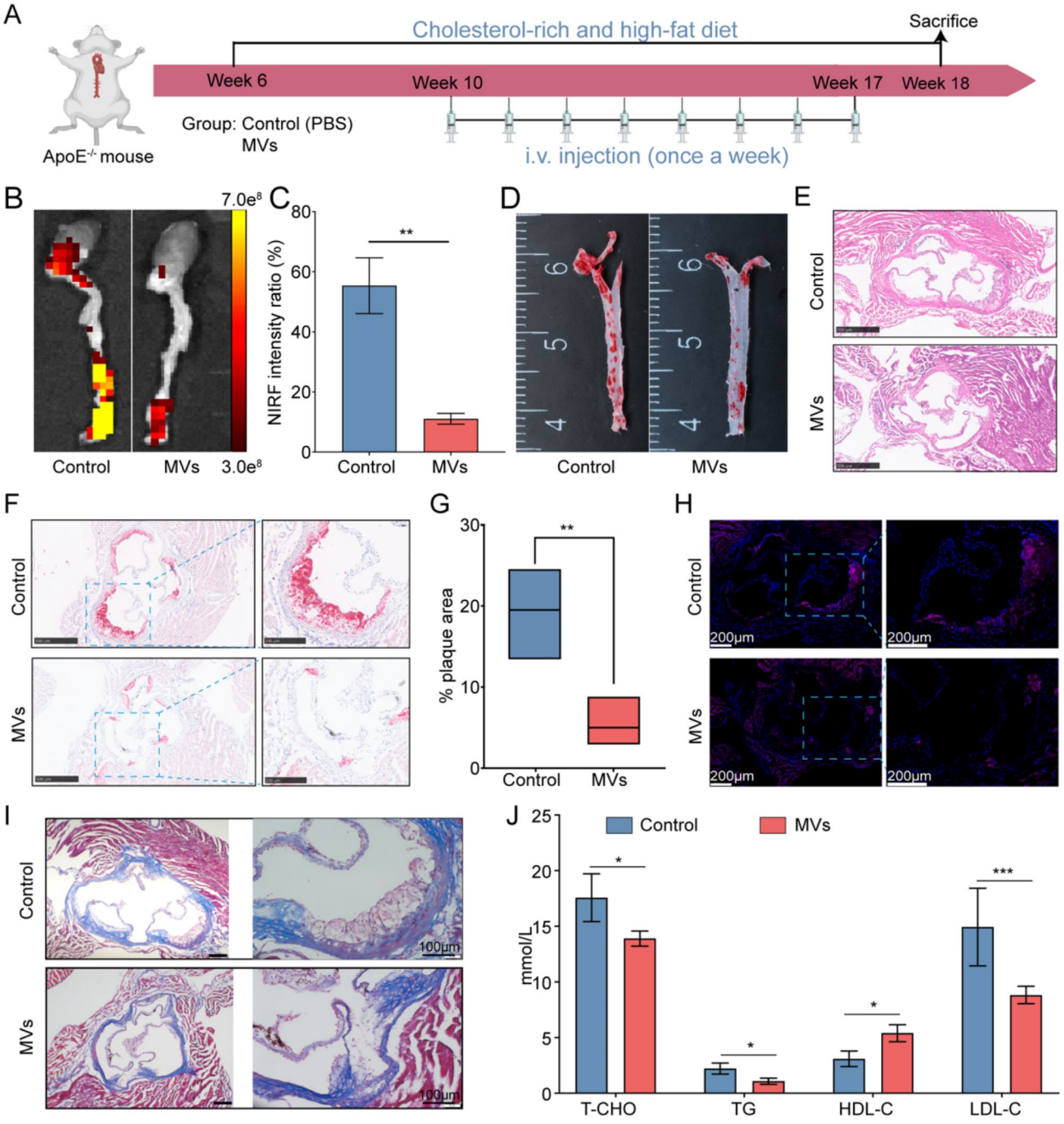

Fig. 3 Therapeutic efficacy of MVs in atherosclerotic mice. (**A**) Schematic representation of the preparation and treatment of atherosclerotic mice. (**B**) Representative ex vivo NIRF images of aortic tissues after the treatment. (**C**) Quantitative analysis of ICG fluorescent signals in the aorta 2 h postinjection. (**D**) Representative photographs of oil red-stained aortas. (**E-F**) HE staining and oil red O staining of atherosclerotic lesions in the aortic sinus in ApoE$^{-/-}$ mice injected with the control treatment or MVs. (**G**) Quantitative analysis of atherosclerotic lesions. (**H**) Fluorescence images showing the accumulation of ICG in atherosclerotic plaques in the aortic root sections of ApoE$^{-/-}$ mice. (**I**) Masson staining of atherosclerotic lesions in the aortic sinus. (**J**) The levels of T-CHO, TG, HDL-C and LDL-C in mice after the various treatments. ($n = 5$, mean ± SD, $^{*}P < 0.05$; $^{**}P < 0.01$; $^{***}P < 0.001$)

collagen levels around the plaques using Masson's trichrome staining, which revealed an increase in collagen concentrations and enhanced fibrous cap thickness in the MVs-treated group (Fig. 3I). Consistent with these findings, the MVs-treated group exhibited reduced serum levels of total cholesterol (T-CHO), triglycerides (TG), and low-density lipoprotein cholesterol (LDL-C), while high-density lipoprotein cholesterol (HDL-C) levels were moderately increased (Fig. 3J).

In vivo safety of MVs treatment

To comprehensively evaluate the safety profile of MVs treatment, we administered 100 mg of MVs to C57BL/6 mice every 10 days for a total of 30 days. The control group received PBS. Our findings revealed several key observations. The body weights in both groups exhibited no significant variations throughout the study period, indicating that MVs treatment did not affect overall body weight (Fig. S2A). Detailed blood analyses, including complete blood counts and clinical chemistry, were conducted. These analyses showed no noteworthy differences between the MVs-treated group and the control group, suggesting that MVs treatment did not induce significant haematological or biochemical abnormalities (Fig. S2B-2E). Hepatic and renal function markers were assessed and showed no signs of hepatic or renal toxicity in either group (Fig. S2F-2 H). Histological examinations, particularly haematoxylin and eosin (H&E) staining, provided further insights. There was no significant evidence of damage or abnormalities in major organs, such as the heart, liver, spleen, lungs, kidneys, or intestines, in either group (Fig. S2I). These findings collectively support the safety and tolerability of MVs treatment in mice, suggesting its potential as a viable therapeutic option.

Mechanisms underlying atherosclerotic plaque regression by MVs

To further explore the underlying mechanism of atherosclerotic plaque regression by MVs, control and MVs-treated foamy macrophages (THP-1 + PMA + oxLDL) were subjected to RNA-seq analysis (Fig. 4A). Principal component analysis (PCA) was used to assess the quality of the RNA sequencing data to ensure its reliability and accuracy (Fig. 4B). The differentially expressed genes induces by MVs treatment are shown in Fig. 4C and include 1705 upregulated genes and 1510 downregulated genes. Among these, the top 50 differentially expressed genes, which include *NCF1*, *HMOX1*, *IL23A*, and *NCF1B*, are shown in Fig. 4D. Furthermore, Gene Ontology (GO) analysis uncovered a plethora of biological processes that are involved in MVs-mediated inhibition of AS, including crucial pathways such as cytokine-mediated signalling and positive regulation of responses to external stimuli (Fig. 4E). Enrichment analyses further shed light on the substantial upregulation of vital biological processes, including but not limited to leukocyte migration, macrophage activation, positive regulation of lipid transport, and lipid export from cells (Fig. 4F). These findings suggest that the inhibition of AS by MVs predominantly involves their capacity to bolster lipid efflux and drive foamy macrophage polarization.

MVs promotes lipid efflux via *NR1H3*-mediated upregulation of *ABCA1*

Our investigation further examined the intricate mechanisms underlying MVs-mediated promotion of lipid efflux and revealed significant insights. KEGG pathway analysis uncovered several pertinent pathways, including TNF signalling, cytokine–cytokine receptor interactions, and lipid and atherosclerosis chemokine signalling. Among these, the "lipid and atherosclerosis" pathway was the most closely related to lipid efflux (Fig. 5A). We then examined the genes within the "lipid and atherosclerosis" pathway that exhibited significant differences (Fig. 5B and Fig. S3). The intersections of these differentially expressed genes with those involved in regulating lipid efflux indicated that *ABCA1* was implicated in MVs-mediated regulation of lipid efflux (Fig. 5C). To validate the potential of MVs to enhance lipid efflux, we subjected foamy macrophages (TO) and MVs-treated foamy macrophages (TV) to oil red O staining, which revealed a concentration-dependent reduction in lipid levels with increasing MVs concentrations (Fig. 5D). To further substantiate these findings, Western blot analysis and RT–qPCR were performed and revealed a proportional increase in *ABCA1* protein and mRNA expression in foamy macrophages with increasing MVs concentrations (Fig. 5E and F). Importantly, the level of *ABCA1* around aortic plaques in the MVs-treated group was higher that in the control group (Fig. 5G).

To determine the regulatory mechanism underlying the upregulation of *ABCA1*, we identified *NR1H3* and *FOXA1* as associated transcription factors through the intersections of differentially expressed genes (Fig. 6A). *NR1H3* upregulation has been reported to enhance *ABCA1* expression, while *FOXA1* may inhibit *ABCA1* expression. Therefore, MVs-mediated promotion of *ABCA1* expression is achieved through *NR1H3* upregulation. The Western blot and RT–qPCR results revealed that the protein and mRNA expression of *NR1H3* increased proportionally with MVs concentrations (Fig. 6B and C). To further confirm MVs-mediated regulation of *ABCA1* via *NR1H3*, we modulated *NR1H3* expression in foamy macrophages by overexpression or knockdown. The results demonstrated that *NR1H3* overexpression increased *ABCA1* protein levels (Fig. 6D and F), while *NR1H3* knockdown reduced *ABCA1* protein levels (Fig. 6G and I). Notably, the combination of *NR1H3* overexpression and MVs treatment failed to enhance *ABCA1* expression. Conversely, the attenuation of *ABCA1* expression caused by *NR1H3* knockdown in foamy macrophages could be effectively reversed by MVs treatment. In summary, MVs upregulate ABCA1 expression through the induction of *NR1H3* expression.

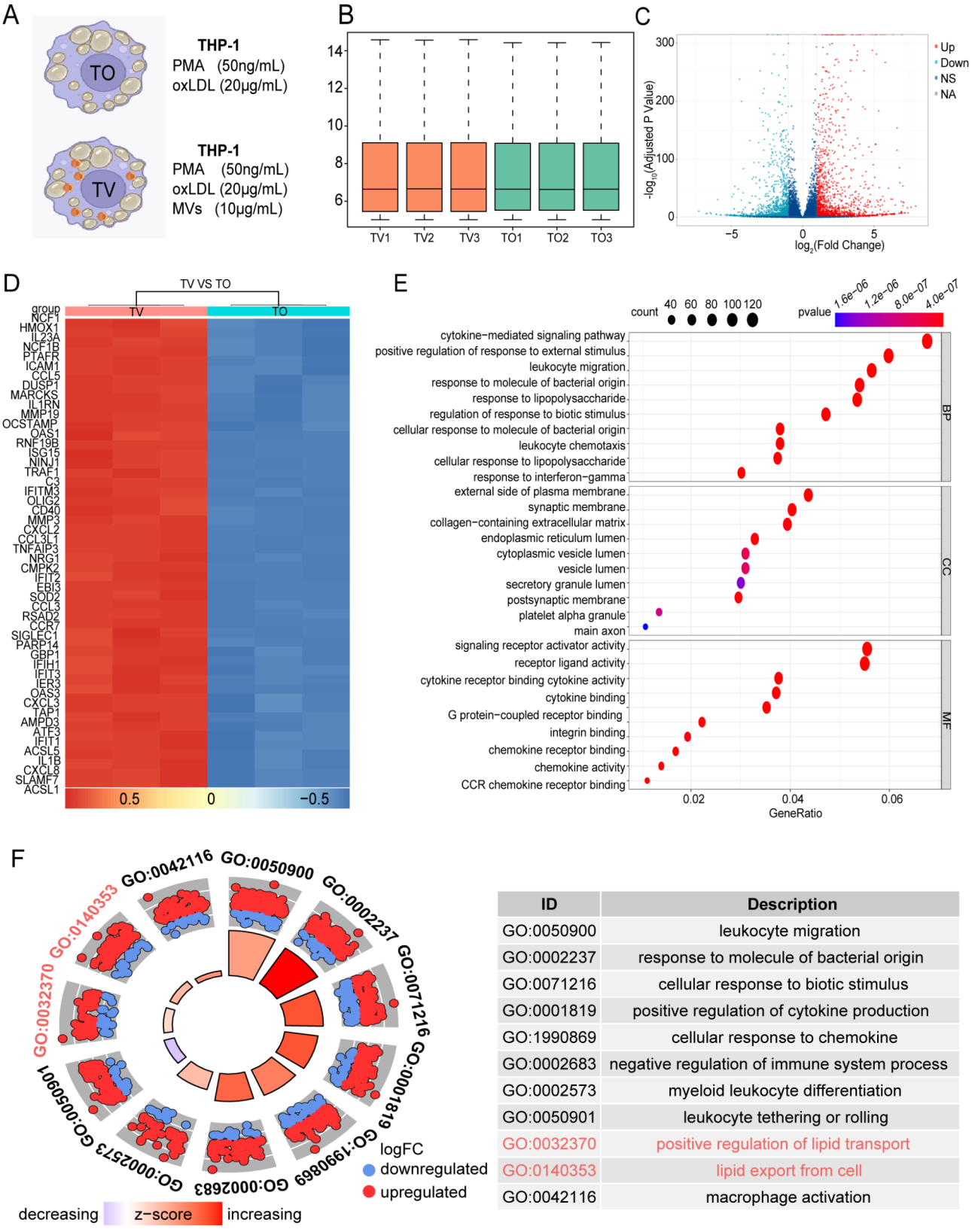

ID	Description
GO:0050900	leukocyte migration
GO:0002237	response to molecule of bacterial origin
GO:0071216	cellular response to biotic stimulus
GO:0001819	positive regulation of cytokine production
GO:1990869	cellular response to chemokine
GO:0002683	negative regulation of immune system process
GO:0002573	myeloid leukocyte differentiation
GO:0050901	leukocyte tethering or rolling
GO:0032370	positive regulation of lipid transport
GO:0140353	lipid export from cell
GO:0042116	macrophage activation

Fig. 4 Bioinformatic analysis of the mechanisms underlying the protective effects of MVs on AS development. (**A**) Schematic diagram of RNA-seq analysis. (**B**) Analysis of the quality control of the RNA sequencing data. (**C**) Changes in the number of genes after MVs treatment. (**D**) Significant changes in the expression levels of genes. (**E**) Alterations in various biological processes following MVs treatment. (**F**) Modifications in biological processes, including the promotion of lipid efflux and the regulation of macrophages, after MVs treatment

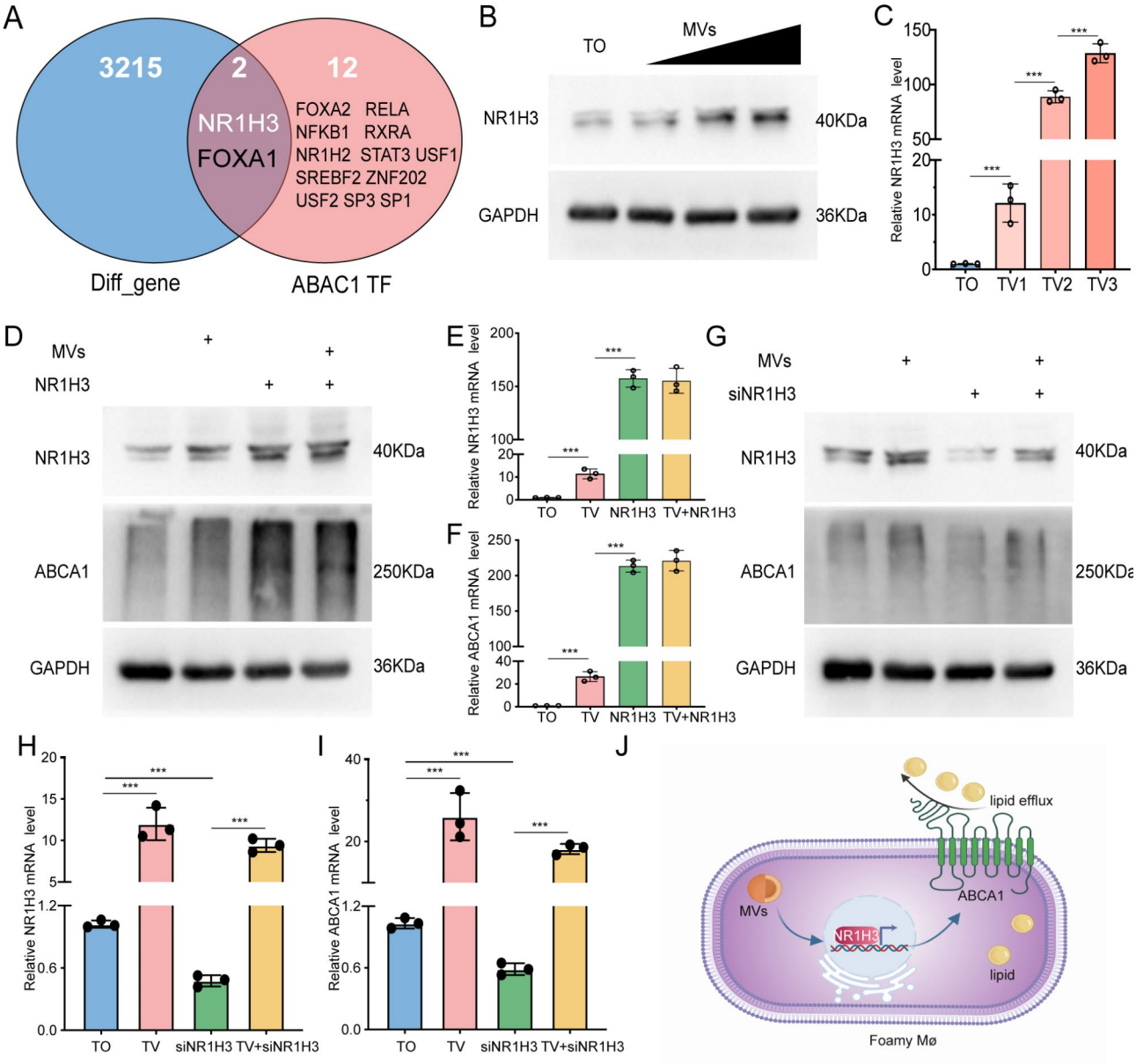

Fig. 5 MVs promotes lipid efflux by altering the expression of ABCA1. (**A**) Significant changes in signalling pathways, including the lipid and atherosclerosis pathways, following MVs treatment. (**B**) Significant alterations in genes involved in the lipid and atherosclerosis pathways. (**C**) Differential genes in the "lipid and atherosclerosis" pathway that intersected with genes that regulate lipid efflux. (**D**) Representative microscopy images of oil red O-stained foamy macrophages treated with various concentrations of MVs (0, 10, 20, 50 μg/mL; TO, TV1, TV2, TV3). (**E-F**) Western blot and RT–qPCR analysis of ABCA1 in foamy macrophages treated with various concentrations of MVs (0, 10, 20, 50 μg/mL). (**G**) Immunohistochemical staining of ABCA1 in aortic tissues after the various treatments (control or MVs). ($n = 5$, mean ± SD, $^{*}P < 0.05$; $^{**}P < 0.01$; $^{***}P < 0.001$)

MVs promote the polarization of macrophages

In addition to enhancing lipid efflux, MVs can induce foamy macrophage polarization (Fig. 7A). RNA-seq analysis revealed he downregulation of several M1 macrophage markers, including *CD86*, *NOS2*, and *TLR4*, following MVs treatment (Fig. 7B). Conversely, several M2 macrophage markers, such as *CD209*, *IL1R2*, and *TGM2*, were upregulated (Fig. 7C). Significant alterations in the levels of various inflammatory factors were observed in response to MVs treatment. The expression of anti-inflammatory factors such as *IL10*, *IL11*, and *IL1RN* was increased, while the proinflammatory factor *IL13* was decreased (Fig. 7D and E). Microscopic examination showed that foamy macrophages exhibited a rounded morphology, while MVs-treated foamy macrophages exhibited an elongated shuttle-like appearance (Fig. 7F). Western blot and RT–qPCR analyses further corroborated these findings, and *CD86* (M1 macrophage marker) was downregulated, while *CD206* (M2 macrophage marker) was upregulated by MVs treatment (Fig. 7G and

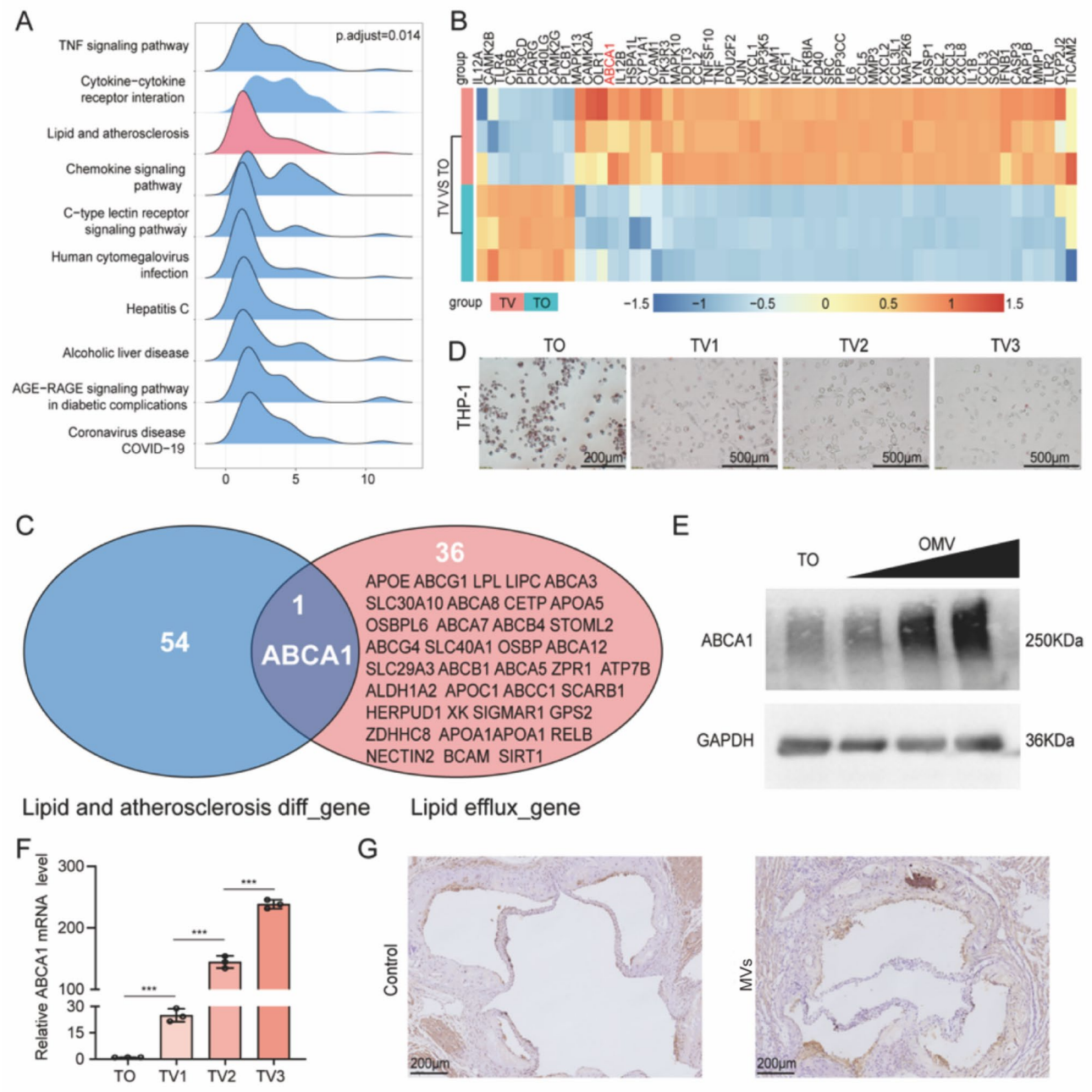

Fig. 6 MVs increased the expression of *ABCA1* by upregulating the transcription factor *NR1H3*. (**A**) Differentially expressed genes obtained by RNA-seq analysis that intersected with transcription factors regulating *ABCA1*. (**B-C**) Western blot and RT–qPCR analysis of *NR1H3* in MVs-treated foamy macrophages. (**D-F**) MVs treatment or NR1H3 overexpression increased ABCA1 protein levels. (**G-I**) *NR1H3* knockdown was reversed by MVs treatment. (**J**) Schematic diagram illustrating the mechanism by which MVs promote lipid efflux. ($n = 5$, mean ± SD, $^{*}P < 0.05$; $^{**}P < 0.01$; $^{***}P < 0.001$)

H). Furthermore, in vitro confocal imaging substantiated these observations, showing a decrease in *CD86* and an increase in *CD206* expression following MVs treatment (Fig. 7I). In vivo, immunohistochemistry confirmed these trends, showing the downregulation of *F4/80* and *CD86* and upregulation of *CD206* (Fig. 7J).

Discussion

In summary, our study introduced a versatile drug delivery vehicle that could modulate lipid metabolism and polarization within foamy macrophages, leading to effective atherosclerotic plaque regression. Unlike existing strategies that rely on PEGylation or antibodies for targeted delivery [25], MVs can be specifically taken up by foamy macrophages within atherosclerotic plaques.

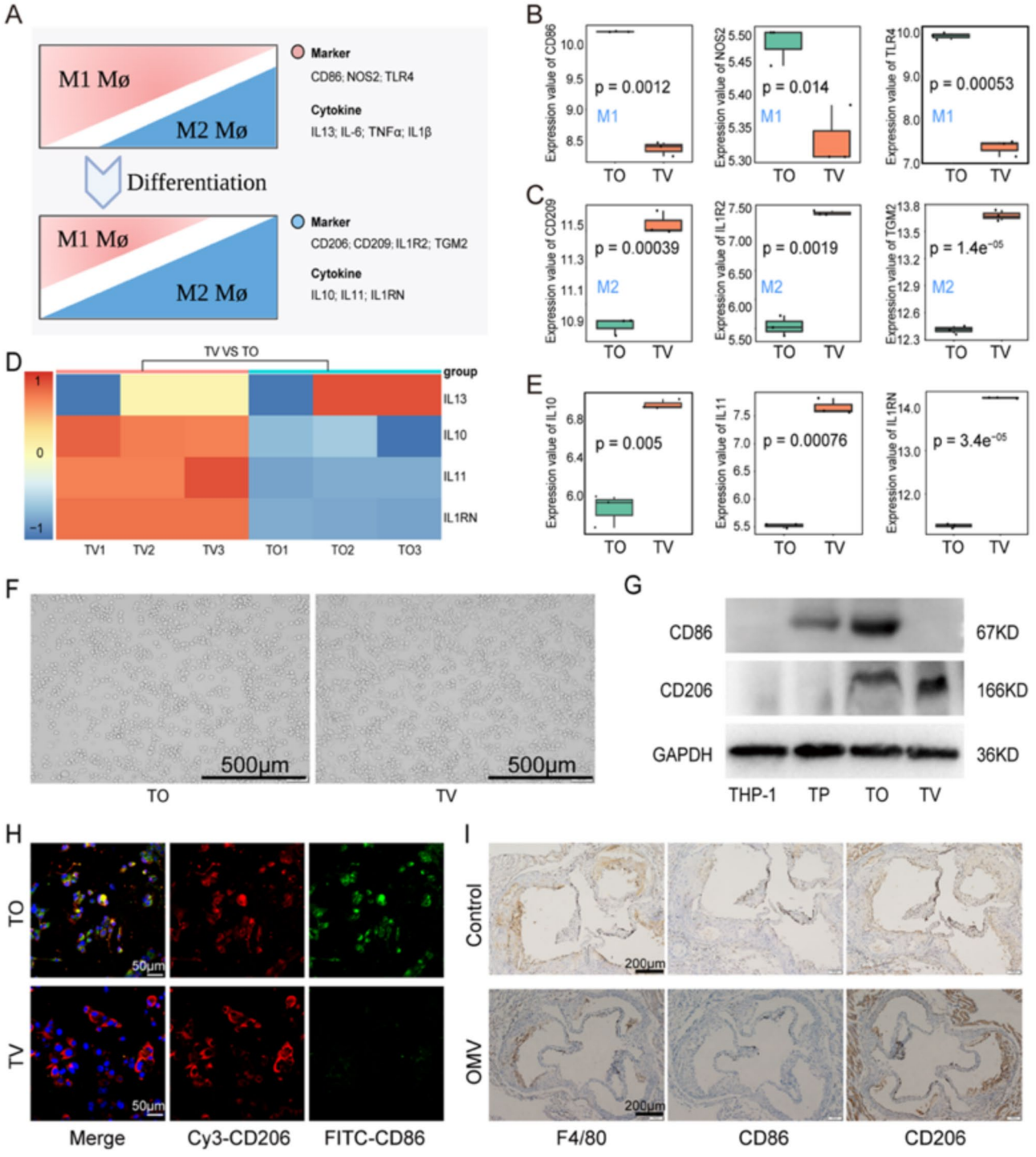

Fig. 7 MVs promote foamy macrophage polarization. (**A**) Schematic diagram illustrating how MVs promote macrophage polarization towards the M2 phenotype. (**B**) The downregulation of M1 markers, including *CD86*, *NOS2*, and *TLR4*. (**C**) The upregulation of M2 markers, including *CD209*, *IL1R2*, and *TGM2*. (**D-E**) The expression of cytokines in foamy macrophages and MVs-treated foamy macrophages. (**F**) Representative microscopy images of foamy macrophages and MVs-treated foamy macrophages. (**G**) Western blot analysis of M1 (*CD86*) and M2 (*CD206*) macrophage markers in foamy macrophages with or without MVs treatment. (**H**) Confocal images showing the expression of M1 (*CD86*) and M2 (*CD206*) macrophage markers in foamy macrophages with or without MVs treatment. (**I**) Immunohistochemical analysis of macrophage (*F4/80*), M1 macrophage (*CD86*) and M2 macrophage (*CD206*) marker expression in aortic tissues after the various treatments (control or MVs). ($n = 5$, mean ± SD, $^{*}P < 0.05$; $^{**}P < 0.01$; $^{***}P < 0.001$)

MVs are naturally and specifically taken up by foamy macrophages within atherosclerotic plaques. This biological nanocarrier harnesses intrinsic cellular functions, eliminating the need for complex targeting molecules or bioconjugation processes. After accumulating in targeted foamy macrophages, MVs promote lipid efflux and macrophage polarization, offering an effective means of AS inhibition. Furthermore, MVs can serve as efficient carriers to deliver various therapeutic agents to atherosclerotic plaques, thereby enhancing overall therapeutic efficacy.

Numerous nanoparticles have been shown to modulate foamy macrophages to treat AS and include polymer nanoparticles, lipid nanoparticles, magnetic nanoparticles, recombinant high-density lipoprotein nanoparticles, and cell membrane biomimetic nanoparticles [26–29]. However, these nanoparticles primarily serve as drug transport carriers and lack inherent therapeutic functions. They often necessitate intricate control over morphology and size, the chelation of targets, drug loading, or the manipulation of external magnetic fields to achieve specific targeting or therapeutic effects. The complex synthesis processes, challenges in batch quality control, and potential toxicity further hinder their widespread clinical use [30].

In contrast, MVs derived from the culture supernatant of oral probiotics offer several advantages, including ease of preparation, enhanced safety, substantial cargo capacity, and high reproducibility [13, 31]. Notably, our study revealed that MVs possess an inherent capability to target and regulate foamy macrophages, which is a characteristic that holds promise for inhibiting the progression of AS. The ability of MVs to target foamy macrophages can be attributed to two key factors. First, MVs exhibit an optimal size (approximately 150 nm) and zeta potential (approximately − 8 mV), which facilitate their passive penetration into atherosclerotic plaques. Second, foamy macrophages are phagocytic cells with a penchant for engulfing dying or dead cells and foreign particles, including microbes [32]. In vitro, flow cytometry and confocal imaging experiments clearly demonstrated the strongest fluorescence signals after the incubation of MVs@ICG with foamy macrophages, underscoring the exceptional binding affinity of MVs to these cells. Furthermore, ex vivo NIRF imaging confirmed the increase in fluorescence signals in aortic tissue and aortic root pathological sections from the MVs@ICG group. Importantly, this fluorescence pattern closely mirrored the distribution of macrophages in the pathological sections, providing conclusive evidence of the remarkable ability of MVs to target foamy macrophages.

MVs can modulate foamy macrophages and inhibit AS, which is crucial in atherosclerotic plaque treatment. Foamy macrophages play a pivotal role in ability of MVs plaque development, and therapeutic strategies often aim to promote lipid efflux and the polarization of these macrophages [5]. This study effectively confirmed the inhibitory effects of MVs on AS through various biological indicators, including ex vivo NIRF imaging of the aorta, oil red O staining of the aorta, oil red O staining of aortic sections, and blood lipid analysis.

Further analysis of the regulatory effects of MVs on macrophages involved two main aspects: enhancing lipid efflux from foamy macrophages and promoting their differentiation into M2-type macrophages. The investigation initially identified *ABCA1* as a significantly upregulated gene associated with lipid efflux. *ABCA1*, which is an integral membrane protein [33], primarily facilitates the transport of intracellular free lipids and phospholipids to extracellular lipid-poor apolipoprotein A-I, leading to the formation of nascent high-density lipoprotein particles [34, 35]. Molecular biology experiments, including Western blot and qPCR, subsequently confirmed that MVs increased the expression of *ABCA1*. To further examine the regulatory mechanisms, we intersected transcription factors associated with *ABCA1* regulation with the differentially expressed genes. The results revealed that MVs regulated *ABCA1* expression through the transcription factor *NR1H3*. To validate this finding, *NR1H3* was overexpressed and knocked down in combination with MVs treatment, which further showed that MVs upregulated *ABCA1* expression by enhancing *NR1H3* activity, ultimately promoting lipid efflux in foamy macrophages.

Additionally, this study observed the downregulation of M1 macrophage markers and upregulation of M2-type macrophage markers through bioinformatics analysis, which was subsequently confirmed by Western blotting, immunofluorescence analysis, and immunohistochemistry. These findings provide valuable insights into the multifaceted effects of MVs on foamy macrophage regulation.

Our data contribute significantly to the understanding of how MVs can effectively regulate macrophages to inhibit AS. Moreover, the versatility of MVs as nanocarriers opens the possibility of loading them with various drugs or combining them with diverse treatment methods, such as sonodynamic therapy, to enhance the efficacy of antiatherosclerotic therapies. These findings hold great promise for advancing our ability to combat atherosclerotic plaques through innovative therapeutic approaches.

Conclusion

The significance of this study lies in its potential to revolutionize the treatment of atherosclerosis by offering a novel and efficient means of targeting and modulating key cellular mechanisms involved in plaque formation. By harnessing the natural properties of MVs, this approach

could pave the way for safer and more effective therapies, addressing the critical need for innovative solutions in combating cardiovascular diseases. This study not only highlights the therapeutic potential of MVs but also sets the foundation for future research into their broader applications in various disease contexts.

Abbreviations

MVs	Probiotic-derived vesicles
NIRF	Near-infrared fluorescence
TEM	Transmission electron microscope
ALT	Alanine amino transferase
AST	Aspartate aminotransferase
ALP	Alkaline phosphatase
BUN	Blood urea nitrogen
CRE	Creatinine
H&E	Haematoxylin and eosin
EPD	Eukaryotic promoter database
GSEA	Gene set enrichment analysis
IL	Interleukin
GM-CSF	Granulocyte-macrophage colony-stimulating factor
PMA	Phorbol 12-myristate 13-acetate
MRS	Man-rogosa-sharpe
DLS	Dynamic light scattering
HDL-C	High-density lipoprotein cholesterol
LDL-C	Low-density lipoprotein cholesterol
TG	Triglycerides
T-CHO	Total cholesterol

Supplementary Information

The online version contains supplementary material available at https://doi.org/10.1186/s12951-025-03360-8.

Supplementary Material 1

Acknowledgements
Not applicable.

Author contributions
B. Jing conceptualized and wrote the article. Y. Gao and L. Wang were responsible for methodology. Y. Bai, M. He, F. Guo, and S. Qin finished formal analysis. D. Jiang and R. An carried out the supervision. M. Xie and L. Zhang carried out the project administration. All authors reviewed the manuscript.

Funding
This study was supported by the National Natural Science Foundation of China (No. 82151316), China Postdoctoral Science Foundation (2022M721262), Free Innovation Pre-research Funding of Wuhan Union Hospital (No. 2022xhyn015) and the Open Foundation of Hubei Provincial Key Laboratory of Molecular Imaging.

Data availability
No datasets were generated or analysed during the current study.

Declarations

Ethics approval and consent to participate
All animal experiments were conformed to the guidelines and standards of the Experimental Animal Center of Tongji Medical College, Huazhong University of Science and Technology.

Consent for publication
Not applicable.

Competing interests
The authors declare no competing interests.

Author details
[1]Department of Ultrasound Medicine, Union Hospital, Tongji Medical College, Huazhong University of Science and Technology, No. 1277 Jiefang Ave, Wuhan 430022, Hubei Province, China
[2]Clinical Research Center for Medical Imaging in Hubei Province, Wuhan 430022, China
[3]Hubei Key Laboratory of Molecular Imaging, Wuhan 430022, China
[4]Department of Nuclear Medicine, Union Hospital, Tongji Medical College, Huazhong University of Science and Technology, Wuhan 430022, China
[5]Department of Pancreatic Surgery, Union Hospital, Tongji Medical College, Huazhong University of Science and Technology, Wuhan 430022, China

Received: 12 August 2024 / Accepted: 31 March 2025
Published online: 16 April 2025

References

1. Moore KJ, Sheedy FJ, Fisher EA. Macrophages in atherosclerosis: a dynamic balance. Nat Rev Immunol. 2013;13:709–21.
2. Libby P, Buring JE, Badimon L, Hansson GK, Deanfield J, Bittencourt MS, Tokgozoglu L, Lewis EF. Atherosclerosis. Nat Rev Dis Primers. 2019;5:56.
3. Ridker PM, Everett BM, Pradhan A, MacFadyen JG, Solomon DH, Zaharris E, Mam V, Hasan A, Rosenberg Y, Iturriaga E, et al. Low-Dose methotrexate for the prevention of atherosclerotic events. N Engl J Med. 2019;380:752–62.
4. Libby P. The changing landscape of atherosclerosis. Nature. 2021;592:524–33.
5. Jinnouchi H, Guo L, Sakamoto A, Torii S, Sato Y, Cornelissen A, Kuntz S, Paek KH, Fernandez R, Fuller D, et al. Diversity of macrophage phenotypes and responses in atherosclerosis. Cell Mol Life Sci. 2020;77:1919–32.
6. Moore KJ, Koplev S, Fisher EA, Tabas I, Bjorkegren JLM, Doran AC, Kovacic JC. Macrophage trafficking, inflammatory resolution, and genomics in atherosclerosis: JACC macrophage in CVD series (Part 2). J Am Coll Cardiol. 2018;72:2181–97.
7. Castano D, Rattanasopa C, Monteiro-Cardoso VF, Corliano M, Liu Y, Zhong S, Rusu M, Liehn EA, Singaraja RR. Lipid efflux mechanisms, relation to disease and potential therapeutic aspects. Adv Drug Deliv Rev. 2020;159:54–93.
8. Liu H, Pietersz G, Peter K, Wang X. Nanobiotechnology approaches for cardiovascular diseases: site-specific targeting of drugs and nanoparticles for atherothrombosis. J Nanobiotechnol. 2022;20:75.
9. Sha X, Dai Y, Chong L, Wei M, Xing M, Zhang C, Li J. Pro-efferocytic macrophage membrane biomimetic nanoparticles for the synergistic treatment of atherosclerosis via competition effect. J Nanobiotechnol. 2022;20:506.
10. Wang Q, Wang Y, Liu S, Sha X, Song X, Dai Y, Zhao M, Cai L, Xu K, Li J. Theranostic nanoplatform to target macrophages enables the Inhibition of atherosclerosis progression and fluorescence imaging of plaque in ApoE(-/-) mice. J Nanobiotechnol. 2021;19:222.
11. Poon C, Gallo J, Joo J, Chang T, Banobre-Lopez M, Chung EJ. Hybrid, metal oxide-peptide amphiphile micelles for molecular magnetic resonance imaging of atherosclerosis. J Nanobiotechnol. 2018;16:92.
12. Khatoon N, Zhang Z, Zhou C, Chu M. Macrophage membrane coated nanoparticles: a biomimetic approach for enhanced and targeted delivery. Biomater Sci. 2022;10:1193–208.
13. Jing B, Qian R, Jiang D, Gai Y, Liu Z, Guo F, Ren S, Gao Y, Lan X, An R. Extracellular vesicles-based pre-targeting strategy enables multi-modal imaging of orthotopic colon cancer and image-guided surgery. J Nanobiotechnol. 2021;19:151.
14. Liang G, Zhu Y, Ali DJ, Tian T, Xu H, Si K, Sun B, Chen B, Xiao Z. Engineered exosomes for targeted co-delivery of miR-21 inhibitor and chemotherapeutics to reverse drug resistance in colon cancer. J Nanobiotechnol. 2020;18:10.
15. Li YJ, Wu JY, Liu J, Xu W, Qiu X, Huang S, Hu XB, Xiang DX. Artificial exosomes for translational nanomedicine. J Nanobiotechnol. 2021;19:242.
16. Jing B, Guo F, An R, Gao Y, Li Y, Xie Y, Wang J, Chen Y, Li H, Gao T, et al. Apoptotic tumor cell-derived microparticles loading Napabucasin inhibit CSCs and synergistic immune therapy. J Nanobiotechnol. 2023;21:37.
17. Guo R, Jiang D, Gai Y, Qian R, Zhu Z, Gao Y, Jing B, Yang B, Lan X, An R. Chlorin e6-loaded goat milk-derived extracellular vesicles for Cerenkov luminescence-induced photodynamic therapy. Eur J Nucl Med Mol Imaging. 2023;50:508–24.

18. Qian R, Jing B, Jiang D, Gai Y, Zhu Z, Huang X, Gao Y, Lan X, An R. Multi-antitumor therapy and synchronous imaging monitoring based on exosome. Eur J Nucl Med Mol Imaging. 2022;49:2668–81.
19. Ren S, Chen J, Guo J, Liu Y, Xiong H, Jing B, Yang X, Li G, Kang Y, Wang C et al. Exosomes from Adipose Stem Cells Promote Diabetic Wound Healing through the eHSP90/LRP1/AKT Axis. Cells 2022, 11.
20. Keshavarz Azizi Raftar S, Ashrafian F, Yadegar A, Lari A, Moradi HR, Shahriary A, Azimirad M, Alavifard H, Mohsenifar Z, Davari M, et al. The protective effects of live and pasteurized Akkermansia muciniphila and its extracellular vesicles against HFD/CCl4-Induced liver injury. Microbiol Spectr. 2021;9:e0048421.
21. Jing B, Gao Y, Guo F, Jiang D, Guo R, Wang J, Li Y, Xie Y, Chen Y, Li H et al. Engineering goat milk-derived extracellular vesicles for multiple bioimaging-guided and photothermal-enhanced therapy of colon cancer. Biomater Sci 2023.
22. Hao H, Zhang X, Tong L, Liu Q, Liang X, Bu Y, Gong P, Liu T, Zhang L, Xia Y, et al. Effect of extracellular vesicles derived from Lactobacillus plantarum Q7 on gut microbiota and ulcerative colitis in mice. Front Immunol. 2021;12:777147.
23. Kim W, Lee EJ, Bae IH, Myoung K, Kim ST, Park PJ, Lee KH, Pham AVQ, Ko J, Oh SH, Cho EG. Lactobacillus plantarum-derived extracellular vesicles induce anti-inflammatory M2 macrophage polarization in vitro. J Extracell Vesicles. 2020;9:1793514.
24. Guo F, Cheng X, Jing B, Wu H, Jin X. FGD3 binds with HSF4 to suppress p65 expression and inhibit pancreatic cancer progression. Oncogene. 2022;41:838–51.
25. She X, Qin S, Jing B, Jin X, Sun X, Lan X, An R. Radiotheranostic targeting cancer stem cells in human colorectal cancer xenografts. Mol Imaging Biol. 2020;22:1043–53.
26. Wang Y, Li L, Zhao W, Dou Y, An H, Tao H, Xu X, Jia Y, Lu S, Zhang J, Hu H. Targeted therapy of atherosclerosis by a Broad-Spectrum reactive oxygen species scavenging nanoparticle with intrinsic Anti-inflammatory activity. ACS Nano. 2018;12:8943–60.
27. Seijkens TTP, van Tiel CM, Kusters PJH, Atzler D, Soehnlein O, Zarzycka B, Aarts S, Lameijer M, Gijbels MJ, Beckers L, et al. Targeting CD40-Induced TRAF6 signaling in macrophages reduces atherosclerosis. J Am Coll Cardiol. 2018;71:527–42.
28. Wang Y, Zhang K, Li T, Maruf A, Qin X, Luo L, Zhong Y, Qiu J, McGinty S, Pontrelli G, et al. Macrophage membrane functionalized biomimetic nanoparticles for targeted anti-atherosclerosis applications. Theranostics. 2021;11:164–80.
29. Sun W, Xu Y, Yao Y, Yue J, Wu Z, Li H, Shen G, Liao Y, Wang H, Zhou W. Self-oxygenation mesoporous MnO2 nanoparticles with ultra-high drug loading capacity for targeted arteriosclerosis therapy. J Nanobiotechnol. 2022;20:88.
30. Sha X, Dai Y, Song X, Liu S, Zhang S, Li J. The opportunities and challenges of silica nanomaterial for atherosclerosis. Int J Nanomed. 2021;16:701–14.
31. Jing B, Gai Y, Qian R, Liu Z, Zhu Z, Gao Y, Lan X, An R. Hydrophobic insertion-based engineering of tumor cell-derived exosomes for SPECT/NIRF imaging of colon cancer. J Nanobiotechnol. 2021;19:7.
32. Zhang J, Zu Y, Dhanasekara CS, Li J, Wu D, Fan Z, Wang S. Detection and treatment of atherosclerosis using nanoparticles. Wiley Interdiscip Rev Nanomed Nanobiotechnol 2017, 9.
33. Attie AD. ABCA1: at the nexus of cholesterol, HDL and atherosclerosis. Trends Biochem Sci. 2007;32:172–9.
34. Westerterp M, Fotakis P, Ouimet M, Bochem AE, Zhang H, Molusky MM, Wang W, Abramowicz S, la, Bastide-van Gemert S, Wang N et al. Cholesterol Efflux Pathways Suppress Inflammasome Activation, NETosis, and Atherogenesis. Circulation 2018;138:898–912.
35. Zheng S, Huang H, Li Y, Wang Y, Zheng Y, Liang J, Zhang S, Liu M, Fang Z. Yin-xing-tong-mai Decoction attenuates atherosclerosis via activating PPAR-gamma-LXRalpha-ABCA1/ABCG1 pathway. Pharmacol Res. 2021;169:105639.

Publisher's note